crystals

MDPI

Article

In-Situ Growth of Nucleus Geometry to Dual Types of Periodically Ringed Assemblies in Poly(nonamethylene terephthalate)

Eamor M. Woo [1,*], Chien-Hua Tu [1,2], Selvaraj Nagarajan [1] and Graecia Lugito [1,3]

[1] Department of Chemical Engineering, National Cheng Kung University, No. 1, University Road, Tainan 701-01, Taiwan; v22032582@gmail.com (C.-H.T.); nagarajan.tech@gmail.com (S.N.); graecia@che.itb.ac.id (G.L.)
[2] Max-Planck Institute for Polymer Research, Ackermannweg 10, D-55128 Mainz, Germany
[3] Faculty of Industrial Technology, Institut Teknologi Bandung, Jl. Ganesha 10, Bandung 40132, Indonesia
* Correspondence: emwoo@mail.ncku.edu.tw; Tel.: +886-6-275-7575 (ext. 62670)

Abstract: Monitoring of nucleus geometry and growth into dual types of periodically ring-banded morphology in poly(nonamethylene terephthalate) (PNT), respectively, Type-1 and Type-2, are done with detailed analyses using polarized-light optical microscopy (POM) in-situ CCD recording; the periodic assembly morphologies are characterized using atomic-force microscopy (AFM) and scanning electron microscopy (SEM). Different annealing treatments (T_{max} = 110, 120, 130 °C) are accomplished at a crystallization temperature of 85 °C; effects on the nucleus geometry, number (25–10%) and volume fractions (33–15%) of Type-2 among two types of banded PNT spherulites are expounded. Growth of a specific type of periodically banded PNT spherulite is initiated from either highly elongated sheaf-like or well-rounded nuclei, with the final grown lamellae being self-packed as multi-shell structures. Nucleation geometry and crystallization parameters collectively lead to development of multiple types of banded PNT spherulites of different relative fractions.

Keywords: ring-banded morphology; poly(nonamethylene terephthalate); lamellar self-assembly

Citation: Woo, E.M.; Tu, C.-H.; Nagarajan, S.; Lugito, G. In-Situ Growth of Nucleus Geometry to Dual Types of Periodically Ringed Assemblies in Poly(nonamethylene terephthalate). *Crystals* **2021**, *11*, 1338. https://doi.org/10.3390/cryst11111338

Academic Editor: Rajratan Basu

Received: 15 October 2021
Accepted: 30 October 2021
Published: 2 November 2021

1. Introduction

In the literature, periodically ring-banded spherulites were widely reported in many polymers, mainly polyesters, such as poly(ethylene adipate) (PEA) [1,2], poly(butylene adipate) (PBA) [3], polyethylene (PE) [4,5], poly(trimethylene terephthalate) (PTT) [6–11], poly(heptamethylene terephthalate) (PHepT) [12], poly(octamethylene terephthalate) (POT) [13], poly(nonamethylene terephthalate) (PNT) [14–17], and poly(dodecamethylene terephthalate) (PDoT) [18]. By contrast, poly(ε-caprolactone) (PCL) displays a dramatically different type of ring bands—termed as acanaceous bands., i.e., with peculiarly rough zig-zag rims and they are not smooth like other ring bands [19–27]. Among the viewpoints, lamellar twisting due to chain-folding stresses [28–32] is a popular model to interpret the formation of banded spherulites; yet, debates on mechanisms and causes for induction of such perplexing periodicity in crystal assembly have been unsettled in the past many decades. In 2012, Woo, et al. [1] initiated a revolutionary approach and first explored the interior lamellar assembly leading to the optically repetitive rings in poly(ethylene adipate) (PEA), and used in-depth analyses to propose mechanistic correlations between the top-surface banding and interior lamellar assembly in the periodically banded aggregates via accurate 3D interior analyses. One single type of ring bands in crystallized polymers is complex enough for long-time controversial debates on searching for mechanisms; some polymers may display not just one type of ring bands but simultaneously two or more types of ring bands in their crystallized aggregates, which make the issue even more complicated. Coexistence of dual types of ring-banded morphology in poly(nonamethylene terephthalate) (PNT), termed as Type-1 (i.e., single ring-banded spherulite) and Type-2 (i.e., double

ring-banded spherulite), was discovered and investigated in prior studies [14–17]. Prior observation on the top surface and internal structures of crystallized PNT has revealed some preliminary yet strong evidence for the detailed lamellar arrangement between the ridges and valleys. Nonetheless, better and more in-depth analyses are necessary to shed light on precise mechanisms. Accordingly, studies [15,16] were conducted on the interiors of two different types of ring bands in PNT intended to better clarify the crystallization and assembly mechanisms of PNT inducing such unusually diversified ring-band patterns.

Unlike most other semicrystalline polymers that usually display a single type of ring bands (when crystallized at a specific temperature within a suitable temperature window), PNT, upon crystallization at a specific T_c, developed two dramatically different types of ring bands (termed as "Type-1 and Type-2") [14,15]. Type-1 PNT bands display entirely different surface-relief periodic morphologies and optical birefringence patterns from Type-2. In-situ monitoring of crystallization and growth from the early stage of nucleation until the final fully grown spherulites (impinged) could be expected to shed light on understanding the mechanisms behind evolution into two different types of ring bands in PNT when crystallized at a specific temperature. A treatment can be applied: heating PNT specimens to a molten state and holding them at a maximum temperature (designated as T_{max}) that is 10–50 °C above their T_m, then rapidly quenching to a fixed T_c and holding them until full crystallization. Upon such annealing treatments, PNT was able to develop two entirely different types of ring bands with various relative fractions depending on T_{max} and T_c. Crystallization at 85 °C was proved for developing known ring-band forms of two different types (Type-1 and Type-2), and it was proven earlier that both Type-1 and Type-2 bands can coexist at any T_c with different relative fractions [14,15]. From these earlier studies, these two types of PNT ring bands are easily distinguishable by their optical birefringence patterns as well as lamellar crystal assemblies.

2. Materials and Methods

Poly(nonamethylene terephthalate) (PNT) was not commercially available; it was synthesized in-house via a two-step polymerization method from monomers: the first process was transesterification, which was then followed by polycondensation [18]. The weight-average molecular weight and the polydispersity index (PDI) of PNT determined by GPC (Waters) using polystyrene as a standard were 28,280 $g \cdot mol^{-1}$ and 1.44, respectively, and thermal analysis revealed $T_g = -2$ °C and $T_m = 92$ °C.

For interior analysis, crystallized PNT films were fractured by pre-cut marking on the glass substrate using a diamond knife to guide the fracture line. The fractured surfaces of the crystallized PNT samples were to be examined using SEM. Fractured surfaces of bulk samples were examined and characterized for revealing a lamellar structure in the fracture and top free surface. Samples in free-standing bulk forms or films cast on glass substrate were fractured across the thickness direction.

Apparatus

Polarized-light optical microscopy (Nikon Optiphot-2, POM). POM was equipped with a Nikon Digital Sight (DS-U1) digital camera, a CCD digital camera (NFX-35) and a microscopic heating stage (Linkam THMS-600 with a T95 temperature programmer); this setup was used to characterize the optical crystalline morphology. In-situ monitoring (for duration up to 48 h) was performed using the CCD camera aided with computer programming. A λ-tint plate (530 nm) was inserted in POM to make contrast interference colors for all POM graphs. PNT film samples for POM were prepared by drop-casting on micro glass slides.

Atomic-force microscopy. AFM (diCaliber, Veeco Corp. Ltd., Plainview, NY, USA, AFM) in intermittent tapping mode with a silicon tip ($f_o = 70$ kHz, $r = 10$ nm) was installed to observe the top-surface topology (phase and height images) as well as for measurement of height profiles.

Scanning electron microscopy.The SEM instrument used was a Hitachi-SU8010, HR-FESEM. The fractured interior and top surface of the specimens were coated with platinum using vacuum sputtering (10 mA, 200 s) prior to SEM characterization. The set-up for mounting the fractured PNT specimens relative to the SEM electron beam (by tilting the sample stand to a pre-determined degree suitable for scanning) was designed to acquire the morphologies of the crystal arrangements on the top surface and fractured interiors simultaneously.

3. Results and Discussion

Figure 1 shows POM micrographs evidencing the relative fractions of Type-1 (i.e., single ring-banded) and Type-2 (i.e., double ring-banded) in PNT crystallized at various T_c = 60–85 °C. T_{max} was fixed at a constant T_{max} = 110 °C. Only Type-1 PNT spherulites (single ring-banded) are present when crystallized at T_c < 85 °C. Type-2 banded PNT spherulite (double ring-banded) appears only at T_c > 85 °C. Both T_c and T_{max} influence the relative abundance of these two types of ring bands, which will be analyzed in detail in following sections.

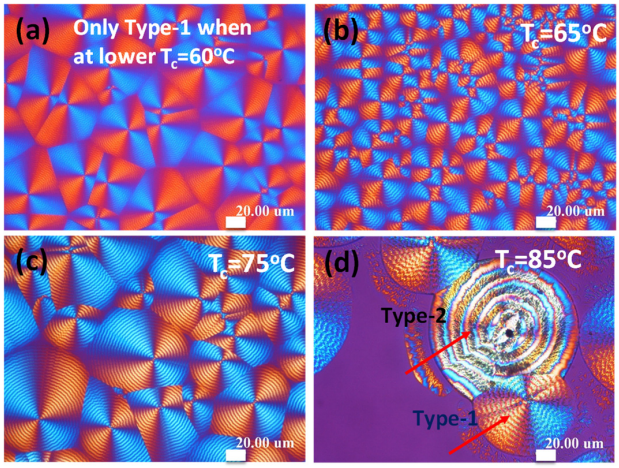

Figure 1. POM micrographs for effects of T_c on relative fractions of dual types of ring-banded spherulites of PNT at T_c = (**a**) 60 °C, (**b**) 65 °C, (**c**) 75 °C, (**d**) 85 °C, (scale bar = 20 μm).

Figure 2 shows POM and OM graphs for effects of T_{max} on the relative fractions of Type-1 over Type-2 banded PNT spherulites upon crystallization at T_c = 85 °C by quenching from different $T_{max.}$ It is noted that the Type-1 and Type-2 morphology remains the same at T_c = 85 °C regardless of changing T_{max}; only the relative fractions of two types vary with T_{max}. By comparing the T_c and T_{max} effects, T_c causes only morphological changes (e.g., double ring-banded spherulites existing in higher T_c regions); however, T_{max} changes the relative percentages of Type-1 vs. Type-2 spherulites. With the T_{max} effects on PNT banded types and their formations, the responsible mechanisms inducing the various fractions of dual types of ring-banded spherulites under a specific T_c are the objective of the subsequent investigation. That is, in general, higher T_c and lower T_{max} (110 °C or lower) are kinetically more favorable for formation of Type-1 bands; oppositely, lower T_c and higher T_{max} (110 °C or lower) are favorable for the formation of Type-2 bands.

In a prior study [33] preceding this current work, influence of crystallization temperature (T_c) on morphology and banding patterns in PNT was investigated in detail; however, the T_{max} effects on the relative fractions of Type-1 vs. Type 2 are yet to be investigated in greater details. A series of different T_{max} were chosen because T_{max} might be one of main factors influencing the formation and growth of banded spherulites. The varying trend of Type-1 vs. Type-2 with the temperature at which the specimens were treated at T_{max} can be clearer if the fractions are plotted as a function of T_{max}. Consequently, T_{max} was varied from 110 to 130 °C, with T_c fixed at a constant 85 °C. Results as a line plot and numerical

values are as shown in Figure 3, which reveal that both volume and number percentages of Type-1 increase with increasing T_{max}. In regard to the fractions of Type-2 spherulites, the trend is just opposite to that of Type-1. The line plots show the variation of the volume and number percentages, respectively, for Type-1 PNT banded spherulites, where (Type-2)% = (100–Type-1)%. The "number%" is counted by the number of spherulites of Type-1 divided by the total number of Type-1 + Type-2, by disregarding the various sizes of individual spherulites. Volume% was estimated by taking into account the actual variations of individual sizes of these two bands. The number percentage of the Type-1 band is always greater than the volume percentage of the same band, as the average size of Type-2 is significantly greater than that of Type-1 (as clearly shown earlier in Figure 2). On the basis of the quantitative results, aided with literature research by Weber, et al. [34], we speculate that the molecular level π-stacking interaction might influence the nucleation process of this Type-2 spherulite. At low T_{max}, higher amount of 'π-π' interaction may be involved in the nucleation process of Type-2 spherulites. At the same time, a higher T_{max} may eliminate 'π-π' interaction in the melt stage, so that the Type-2 spherulite's volume and number percentages might decrease.

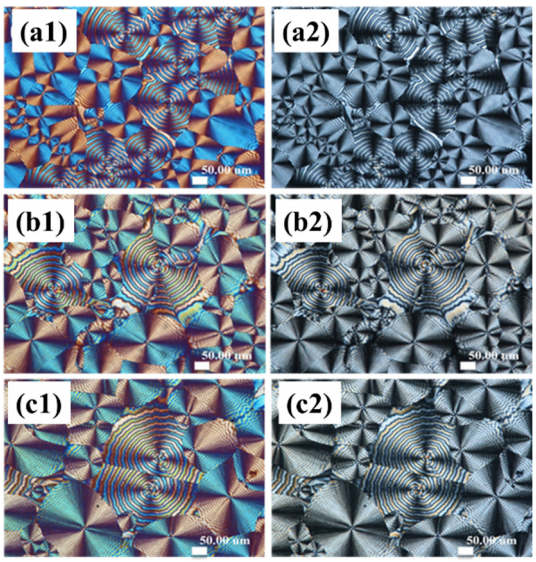

Figure 2. (**a1**,**b1**,**c1**) POM with tint plate and (**a2**,**b2**,**c2**) POM without tint plate graphs showing effects of T_{max} on relative fractions of Type-1 over Type-2 bands in PNT spherulites crystallized at T_c = 85 °C by quenching from different T_{max}: (1) 110 °C, (2) 120 °C, (3) 130–140 °C, (scale bar = 50 μm).

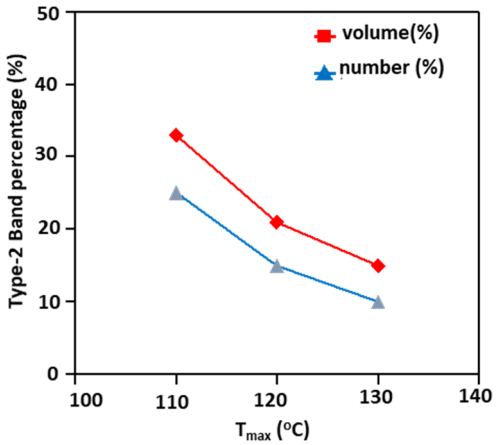

Figure 3. Plot for the variation of volume and number percentages for Type-2 spherulites. [Type-1]% = (100 − Type-2)%.

When melt occurs at a higher T_{max} (but crystallized at a fixed T_c), the shape and geometry of the nuclei might be altered, which leads to variation in banded PNT spherulites. As the density and geometry of the nuclei are different after being soaked at different T_{max}, the fact that Type-1 spherulites always are more dominant in number percentages over Type-2 at any T_c [33] suggests that the nucleus density might be different at various T_{max} or T_c. If T_{max} is kept at 120 °C, then a higher T_c (above 80 °C) favors formation of higher fractions of Type-2 banded spherulites; vice versa, a lower T_c (below 80 °C) leads to smaller volume/number fractions of Type-2 and favors formation of Type-1 banded spherulites. Thus, the crystallization kinetics that might collectively govern the formation of two different types of banded PNT spherulites were probed and analyzed, as discussed above.

The growth rates of Type-1 and Type-2, respectively, are compared as shown in Figure 4. Results show that there is no significant difference in the spherulites growth rates between them. The initiation times (or incubation of first traces of nuclei) for Type-1 and Type-2 are dramatically different. It takes a much longer time for the first traces of nuclei of Type-2 to appear and to initiate growth than that for nuclei of Type-1. This explains that the percentages of Type-1 are in general higher than that of Type-2 under most kinetic environments. In general, growth rate depends on chain diffusion; at 85 °C molecular diffusion is the same for both the spherulites. Further, a Type-1 spherulite may nucleate from an aliphatic segment, and Type-2 nucleation may evolve from the aromatic segment. These two different nucleation environments may result in morphological difference between Type-1 and Type-2. Further, possibility of 'π-π' interaction at higher T_{max} is low, so that Type-2 spherulite percentage is less at T_{max} = 130 °C.

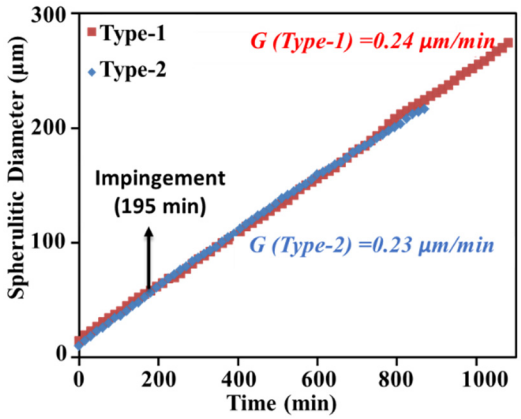

Figure 4. Growth rate of Type-1 and Type-2 spherulites crystallized at T_c = 85 °C by quenching from T_{max} = 120 °C, nucleus state to form in 2 h for Type-1 spherulite 20 h for full-crystallization and for Type-2 spherulite 17 h for full-crystallization.

From the very beginning of initiation of nuclei, Type-1 crystals differ from Type-2. The Type-1 nuclei are of a uniquely asymmetric stick-like geometry. Subsequent growth much follows the initial asymmetric geometry of Type-1 nuclei; thus, the differential variation in the geometry of nuclei may be critical to induce the diversification of the final banded morphology. Schematics for growth evolution are as depicted in Figure 5. The schemes, justified by the experimental POM in-situ monitoring results, indicate that at 85 °C nucleation is initiated, followed with two dramatically different types of nuclei and these nuclei respectively grow and crystallize into final Type-1 and Type-2 ring-banded PNT spherulites. These two different types of nucleus geometries finally evolve into Type-1 (grown from sheaf-like nuclei) and Type-2 (from well-rounded nuclei) ring-banded spherulites at t = 4 h, respectively. Thus, the types (1 or 2) of ring bands in PNT spherulites are determined by the geometry of nuclei at the initial nucleation stage, and in the later stage of growth the patterns of ring bands would be fixed and do not change further upon crystallization and growth; they may simply grow to larger sizes by following the initial nuclei as coded templates. The growth rates of Type-1 and Type-2 are even quite

comparable (refer to earlier Figure 4), differing only in the initial nucleus geometry and lamellae assembly in final fully grown spherulites. The bottom graph (b-1) of Figure 5 shows schematics exemplifying the rod-like nuclei growing into Type-2 ring bands. The spiral patterns (either mirror-image symmetric spiral or an Archimedean single spiral) of the ridge lamellae will be further exemplified by AFM and SEM analyses in later sections.

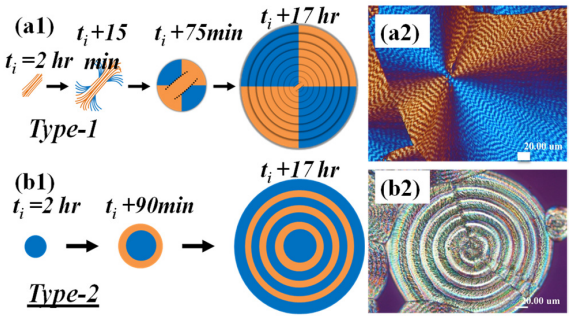

Figure 5. Schematic illustrations and POM graphs for morphology evolution of (**a1**,**a2**) Type-1 in comparison with (**b1**,**b2**) Type-2 spherulites crystallized at T_c = 85 °C by quenching from T_{max} = 120 °C after 2 min.

In-Situ Growth Monitoring

Co-existence of two nuclei geometry shapes at initiation of crystallization held at T_c = 85 °C is thus quite apparent, showing two types of nuclei (t = 2 h at T_c = 85 °C): (1) highly elongated sheaves, and (2) well-rounded nuclei. Figure 6 shows in-situ POM with CCD monitoring on the initiation stages of morphology evolution of Type-1 and Type-2 spherulites, both being crystallized at T_c = 85 °C, from t_i (2 h) to t_i + 120 min (ca. t_i + 2 h). The nuclei for Type-2 and Type-1 banded PNT spherulites are tiny and discrete, but of distinctly different geometric shapes. They are marginally distinguishable in their unique optical birefringence characteristics. The nuclei for Type-2 are initially well-rounded, appearing as a tiny dot-like aggregate. By contrast, the nuclei for Type-1 are highly asymmetrically elongated-rod-like, appearing as a stick-like sheaf with a single birefringence color (orange color), which means that the crystal sheaf-bundle is initially in only one orientation. When fully grown, the highly asymmetric nucleus center for the Type-1 band eventually leads to an asymmetrically packed banded spherulite, as proved in an earlier study.

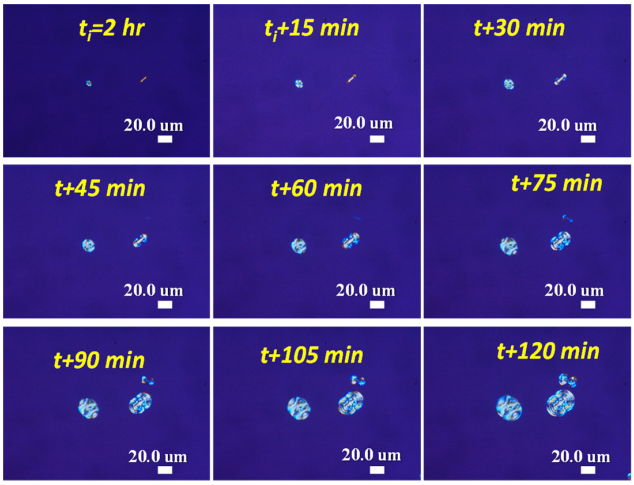

Figure 6. In-situ POM graphs for initial stages of morphology evolution of Type-1 and Type-2 PNT spherulites crystallized at T_c = 85 °C by quenching from T_{max} = 120 °C.

It should be noted, though, that the "incubation time" (time for nuclei to first appear), defined as the time for the first appearance of traceable nuclei after equilibrilating at T_c, for different types of banded PNT spherulties varies dramatically, which means that the initial nuclei for different banded spherulites may appear at different times after being quenched from the molten state at T_{max} to T_c for crystallization. The lamellar assemblies of PNT being packed into different birefrigent patterns of Type-1 and Type-2a,b banded spherulites will be discussed in details later. Figure 7 shows that by quenching the PNT melt from T_{max} = 120 °C to crystallization at T_c = 85 °C, the nuclei (well-rounded shape) for Type-2 (double-ring banded including Type 2a and Type 2b) spherulites appear almost immediately upon equilibrating at T_c = 85 °C; by contrast, it takes about 45 min after equilibrating at T_c before first traces of nuclei (elongated sheaf-like lamellae) for Type 1 banded spherulites appear. One can easily see from the in-situ POM results in Figure 7a–k that although the sheaf-like nuclei (For Type-1 banded spherulites) appear later than those well-rounded ones for Type-2, the nuclei density of the elongated sheaf-like nuclei, once formed, are more densely populated than the well-rounded nuclei whose number density stays almost unchanged with time. This fact leads to eventually higher volume/number fractions of Type-1 over Type-2 banded spherulites when crystallization is completed at any given T_c. Apparently, higher T_c is favorable for greater fractions of Type-2 (over Type-1), but higher T_{max} tends to decrease it as higher T_{max} supposedly suppresses more Type-2 nuclei. Moreover, all these factors (T_{max} and T_c) possibly govern the relative fractions of different types of banded PNT spherulites at the nucleation stage, but not during the spherulites' growth period as the growth rates are almost the same for different types of banded spherulites. Figure 7l shows that that fully grown Type-1 crystals are smaller than the Type-2 ones, and both types mutually impinge on each other. The POM images clearly indicate that two different types of ring bands evolve and grow independently from two geometrically different nuclei, where Type-1 ring-banded PNT spherulites (marked with red arrow) grow from elongated rods nuclei and Type-2 mirror-paired ring-banded spherulites (marked with green arrow) grow from initially well-rounded dot-like nuclei.

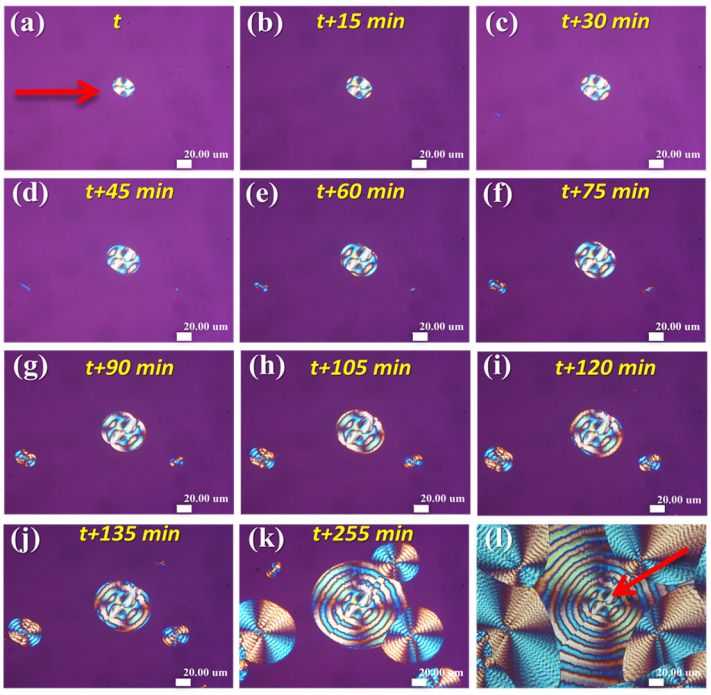

Figure 7. POM graphs of PNT Type-2 in-situ growth captured at T_c = 85 °C after being quenched from T_{max} = 120 °C for different time of crystallization" (**a**) t_o = 2 h, (**b**) t_o + 15 min, (**c**) t_o + 30 min, (**d**) t_o + 45 min, (**e**) t_o + 60 min, (**f**) t_o + 75 min, (**g**) t_o + 90 min, (**h**) t_o + 105 min, (**i**) t_o + 120 min, (**j**) t_o + 135 min, (**k**) t_o + 255 min, (**l**) t_o + 1 day (fully grown). (scale bar = 20 μm).

Note that at T_c = 85 °C, it took quite long times for the first traces of nuclei to appear: for the rod-like nuclei, t_i = 2 h; for the well-rounded nuclei, t_i = 4 h. That is, not only thegeometry shapes differ significantly, but also the times of "incubating" the first traces of nuclei are also different dramatically (t = 2 h vs. 4 h for Type-1 and Type-2 respectively). Apparently, the types (either Type-1 or -2) of ring bands in PNT spherulites are mostly determined by the initial geometry of the nuclei at the nucleation stage, and patterns of ring bands were fixed and did not change further upon crystallization and growth, leading to the final Type-1 vs. Type-2 ring bands. These two different geometries of nuclei both grow eventually to ring-banded PNT spherulites, which differ significantly in their optical birefringence pattern and lamellar assembly.

Depending on the sites of nucleation (near top surface or bottom substrate), crystallized PNT may take a different geometry of banded structures. Figure 8 shows that the nuclei of Type-1 PNT banded spherulites (T_c = 85 °C), at the very center of the periodic bands, take an asymmetric sheaf-like geometry. The lamellae grow along the sheaf direction and spray out like a fan; and upon growing outward, they periodically wave up and down. By contrast, along the perpendicular direction normal to the bundled sheaf, the lamellae are packed as layered plates pointing vertically to the paper, which upon fracture, display some ductile textures. Thus, the lamellae are self-assembled in an asymmetric pattern with respect to the nucleus center. Along the sheaf-crystal direction, the lamellae are mostly flat-on on the paper, other than waving up and down. The lamellae in the perpendicular direction to the nucleus sheaf point to a normal direction to the paper. Owing to the highly elongated nucleus geometry and subsequent directional growth, the interior lamellae in fully grown Type-1 banded spherulites are not circularly symmetric, but highly asymmetric to display two-face dissymmetry in its interior lamellae assembly as revealed in an earlier study [33]. Obviously, the structured and oriented growth from sheaf-like nuclei lead to a highly asymmetric morphology in poly(nonamethylene terephthalate) (PNT) upon packing into periodic bands [24].

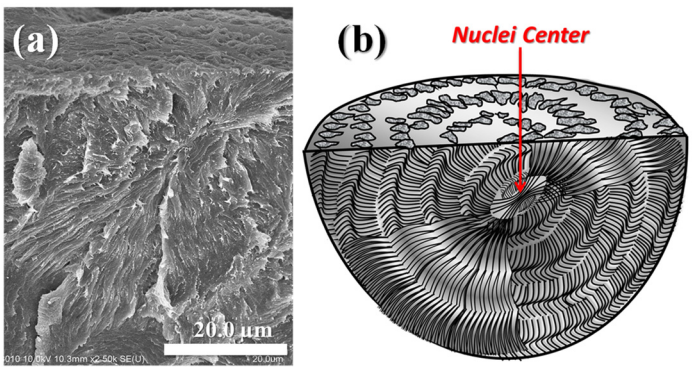

Figure 8. Asymmetric growth from the nucleus in Type-1 PNT ring bands: (**a**) SEM graph for interior, (**b**) schematic for asymmetric assembly around the nuclei in Type-1 banded spherulite (2500×). (Reprinted with copyright permission [33]).

As described in detail in the scheme (Figure 8b), the two tail-ends of rod-like nucleus-sheaves first evolve needle-like fine lamellae that bend into curvature as they grow outward from the ends. Eventually, the bent lamellae grow in a spiral-spin pattern into ridges (aligned circumferentially), then from which daughter branches further grow in the perpendicular direction (i.e., aligned radially) to fill the inter-ridge space. Cycles repeat in the same manner until drainage or impingement.

Figure 9 shows in-situ POM-CCD monitoring on the intermediate stages of the morphology evolution of Type-1 and Type-2 spherulites crystallized at T_c = 85 °C, from t_i + 135 min (ca. 2 h) to t_i + 255 min (ca. 4 h). Type-2 and Type-1 banded PNT spherulites are discrete and distinguishable in their unique optical birefringence characteristics. They are ca. 60–80 μm in diameter, and both become oval-shape (Type-1) or well-rounded (Type-2).

At the intermediate stage, the initially asymmetric stick-like nuclei of Type-1 now grow into oval-shape spherulites with visible optical bands. The initially well-rounded dot-like nuclei for Type-2 still retain a ball-like shape but grow into bigger round-shape spherulites with similar visible optical bands as those in Type-1.

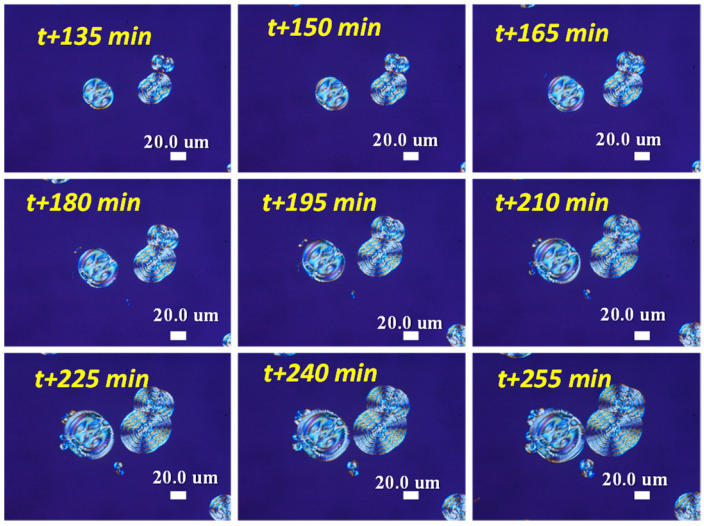

Figure 9. In-situ POM graphs for intermediate stages of morphology evolution of Type-1 and Type-2 spherulites crystallized at T_c = 85 °C by quenching from T_{max} = 120 °C.

Figure 10 shows in-situ POM monitoring on the later or final stages of morphology evolution of Type-1 and Type-2 spherulites crystallized at T_c = 85 °C from t_i + 675 min (ca. 11 h) to t_i + 795 min (ca. 13 h). Type-2 banded PNT spherulites are now fully grown but severely impinged with the neighboring Type-1 banded spherulites. Population of Type-1 banded aggregates dramatically out-numbers that of Type-2 ones.

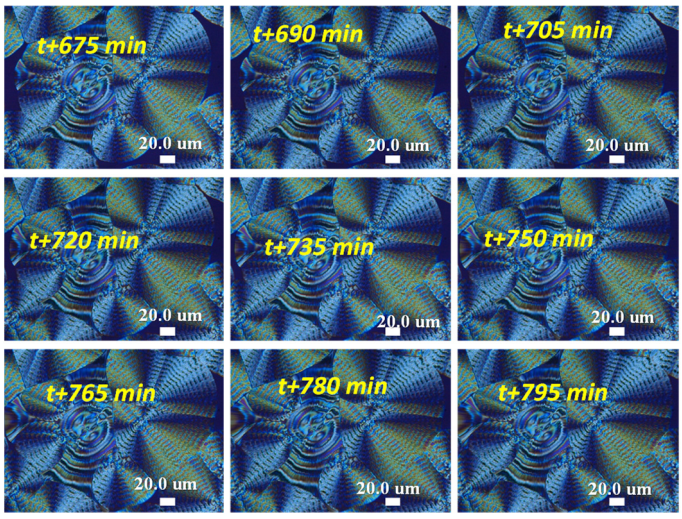

Figure 10. In-situ POM graphs for later or final stages of morphology evolution of Type-1 and Type-2 spherulites crystallized at T_c = 85 °C by quenching from T_{max} = 120 °C.

Figure 11 shows AFM height images and height profiles for Type-1 (left column of images) in comparison with Type-2 (right column of images) PNT spherulites fully crystallized at T_c = (a) 75, (b) 80 and (c) 85 °C by quenching from T_{max} = 120 °C. The nuclei centers of both types of PNT ring bands are located at the lowest regions of the entire banded spherulites of either Type-1 or Type-2. As the spherulites grow away from the nucleus, periodic bands develop, with corresponding heights up and down at ridge

and valley, respectively. The height drops from the ridge to valley are greater for Type-2 bands than for the Type-1 bands. In addition, the inter-band spacing for a Type-2 band is 2–3 times larger than that for a Type-1 band. That is, the surface characteristics of the Type-1 PNT band differ dramatically from those of Type-2.

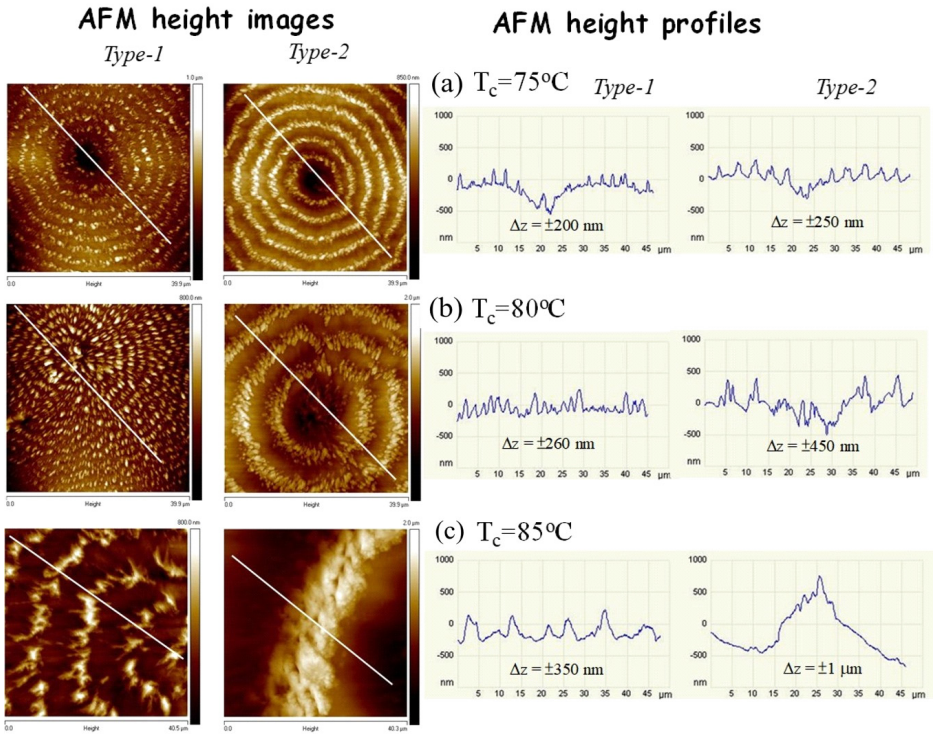

Figure 11. AFM height images and height profiles for Type-1 and Type-2 PNT spherulites fully crystallized at three different T_c = (**a**) 75 °C, (**b**) 80 °C, (**c**) 85 °C, by quenching from T_{max} = 120 °C. (Reprinted with copyright permission [17]).

For universal comparison, additional PNT specimens crystallized at T_c = 80 °C were similarly analyzed using AFM using procedures reported in a previous work [16]. Figure 12 shows (a) POM graph and (b) AFM height images for Type-1 and Type-2 PNT spherulites fully crystallized at T_c = 80 °C until completion, after quenching from T_{max} = 120 °C. Figure 12c,d shows the AFM height profiles for Type-1 and Type-2, respectively. The main characteristics for PNT specimens crystallized at T_c = 80 °C are similar to those crystallized at either lower T_c = 75 °C or higher T_c = 85 °C. The nuclei center is consistently the lowest region of the entire banded spherulites, either of Type-1 or Type-2. Away from the nucleus center, the AFM height profiles (Figure 12c) for Type-1 and Type-2 both show periodic heights waving up and down. The height drops from the ridge to valley are greater for the Type-2 bands than for the Type-1 bands. In addition, both POM and AFM results indicate that the inter-band spacing for a Type-2 band is visibly much larger than that for a Type-1 band. All these features clearly indicate that these are two different types of PNT bands.

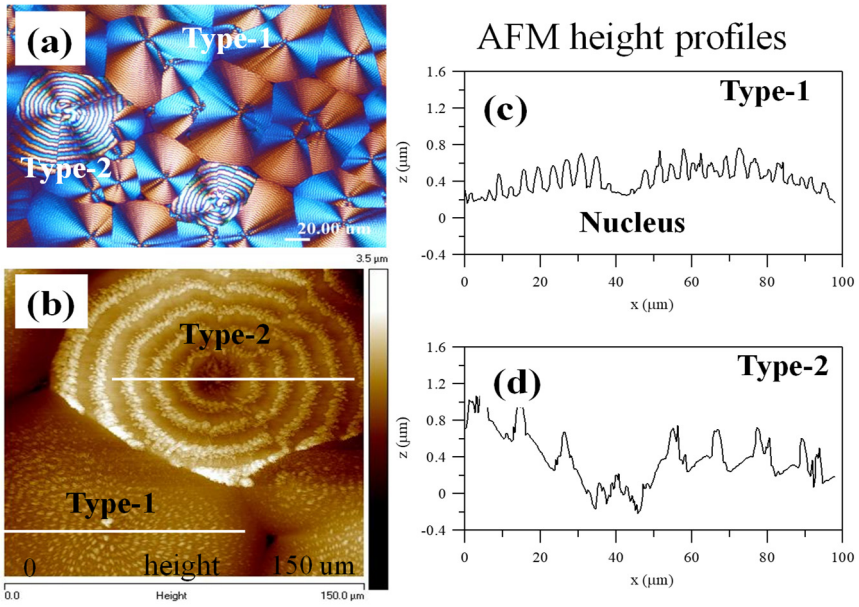

Figure 12. (**a**) POM, and (**b**) AFM height images and (**c**,**d**) height profiles for Type-1 and Type-2 PNT spherulites, respectively, both fully crystallized at T_c = 80 °C by quenching from T_{max} = 120 °C. (Reprinted with copyright permission [16]).

The correlation of the top surface with the fractured surface of Type-1 spherulite with the nuclei center near the interface (polymer/air) was analyzed in detail in an earlier work [33]. Crystallized Type-1 PNT spherulites were dissected by fracturing the specimens with different nucleus positions relative to the bottom substrate or top surface to see whether or not there may be any discrepancy in its interior lamellar arrangement. Figure 13a–c shows SEM graphs of the top surface and interiors of Type-1 banded spherulites with nuclei near the top surface (i.e., interface of polymer/air), which reveal that the crossbar pitch of the interior grating structure tends to be same or similar to the inter-band spacing on the top surface. In addition, the ridge on the top surface can be correlated directly to the protruded ductile fracturing zones while the valley on the top surface is correlated to the convex brittle detaching zones. The periodic ductile fracturing zones suggest that the lamellae in those zones are oriented "along" the fracturing direction, while brittle detaching, next to the ductile pull-out, indicates that the lamellae in the brittle zones are oriented perpendicularly to the fracturing direction. The alternate ductile-brittle failures in the interior lamellae give a hint that the interior lamellae are aligned in an alternate tangential/radial direction, forming a grating architecture in the interiors that are correlated with the periodic up-and-down topology of the ridge and valley bands on the top surface. The crossbar pitch of the interior periodic gratings is ca. 7 μm (as revealed in SEM), which is the same as the inter-band spacing of 7 μm on the top surface as revealed in POM results, whose main characteristics of periodicity are shown in the schematic of Figure 13d.

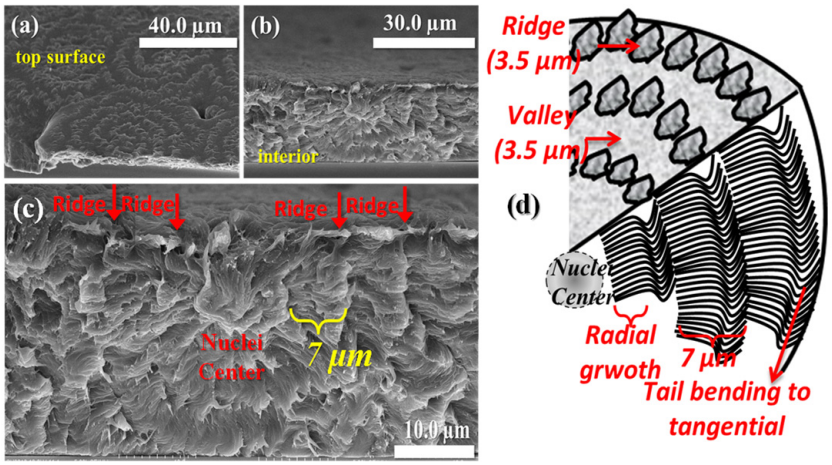

Figure 13. SEM graphs for (**a**) top surface and (**b**) correlated interior lamellar arrangement, and (**c**) zoom-in (6000×) image of (**b**) Type-1 PNT spherulites with the nucleation center near the top surface, (**d**) scheme for interior grating assembly correlating to top surface bands. ((**c**)-reprinted with copyright permission [33]).

Two kinds of discontinuities in lamellar arrangement are present in the interior lamellae assembly of Type-1. The lamellae of Type-1 spherulites demonstrate the different arrangements upon being observed from different dissection angles; in addition, the nuclei positions either near the top surface or more inside the spherulite influence the final arrangement and complexity of the interior lamellae. With regard to Type-2 spherulites of PNT, strong correlation between the topography and interior lamellar assembly is observed; that is to say, both the lamellar arrangement on the top surface and inside the bulk display similarly lamellar-tilted characteristics. More interestingly, the interior lamellae of Type-2 spherulites clearly demonstrate the periodically tail-bending and twisting nature when the sample thickness is increased to a certain level; however, with film thickness decreases to sub-microns and nano-meters, such bending and twisting nature is no longer present, eventually leading to non-periodic or ring-less assemblies.

Earlier investigation [35] has revealed the detail morphologies of Type-2 PNT aggregates, which have two morphologies, and are sub-divided into two categories. Once again, their respective nucleus morphologies are assessed. Figure 14a,b shows schematics of evolution from the nucleation stage to fully grown spherulties of Type-2a vs. Type-2b PNT ring bands. As discussed earlier, Type-2 ring bands further differ in geometric shapes and can be sub-divided into two categories (Type-2a and -2b). Further analyses will expound in more detail on lamellar architectures of the "mirror-pair ring (Type-2a)" and "Fermat's spiral ring-banded (Type-2b)" PNT spherulites. The corresponding schematics for Type-2a and 2b are drawn in the right diagram of the figure to differentiate the specific differences in the morphologies of these two types of banded PNT spherulites. Type-2a and Type-2b banded PNT spherulites both originate from nuclei of a well-rounded shape, but they are different in the birefrigent patterns, which lead to variation of subsequent lamellar growth orientations. For the mirror-paired ring-banded PNT spherulites (Type-2a), as shown in Figure 14a, the polymer crystals start to grow concentrically from the nucleus regions with symmetrical arrangements (mirro-image). The Fermat-spiral ring-banded PNT spherulites (Type-2b) are shown in the right-hand-side scheme of Figure 14b, where the spiral-shape nuclei are initially formed first, to be followed by two crystal arms growing out from the tips of the spiral nuclei, then further grow to fully fill the entire space of the spherulite. It is noteworthy to mention that Type-2a is more abundant but Type-2b spherulites occur only sporadically; sometimes there is no or only a trace amount of Type-2b spiral-banded spherulites in a fully-crystallized PNT sample at T_c = 85 °C. Such morphologically sporadic occurrence of the spiral-spin band patterns was discovered as documented in the literature in PE [36], PCL [20], PDT [37] and PTT [38]. However, interpretation of supercooling effects

on the formation of Type-2b PNT spherulites is not certain and still needs to be confirmed in future work. From the clear microscopic evidence on interior anatomy as shown, the growth in either types of banded PNT spherulties definitely cannot be described as a lamellar plate undergoing synchronized helix-twist from the nuclei center to periphery of spherulites, as claimed by overly simplified classical models of continuous helix-twisting lamellae [35]. Note here that interior 3D-dissected morphology for PNT Type-2 banded spheruites (which are further classified into two sub-classes: Type-2a and Type-2b) were analyzed in detail in a previously published paper [35]; thus, we do not elaborate on the issue here.

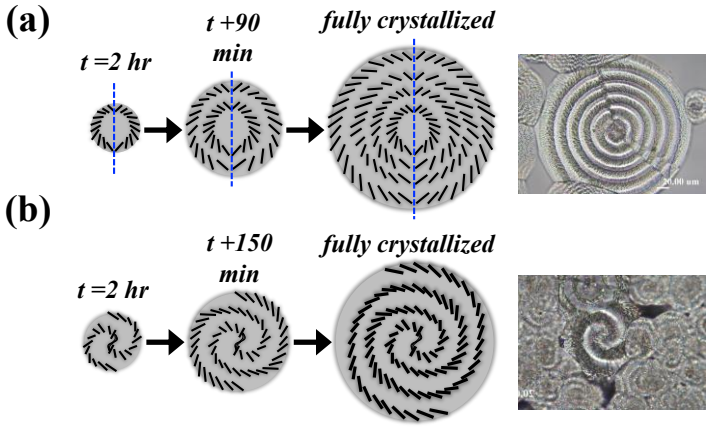

Figure 14. Schematics justified with OM images for in-situ morphological evolution of (**a**) Type-2a mirror-paired ring-banded, (**b**) Type-2b Fermat's-spiral ring-banded PNT spherulites upon crystallization at T_c = 85 °C after quenching from T_{max} = 120 °C held for 2 min.

Spiral-spin growth from a nucleus center appears to be quite universal in polymer spherulites with periodic ring bands. It is worthy to mention that poly(L-lactic acid) (PLLA) also displays similar spiral-spins from its nucleation center, forming multiple types of assemblies with periodic aggregates [39]. Based on the dissected microscopic evidence on the Type-1 ring-banded PLLA spherulites, the growth starts with sheaf-like nuclei, which from two ends would twist and bend, then continue into a full-length double-spiral (or mathematically a "Fermat's spiral"). The result is formation of a concave U-shape valley between two successive lamellae spirals, where the branching lamellae constitute the parallel lamellae underneath the "valley band", leading to a periodic grating architecture. Such grating structure in the ringed PLLA spherulite is quite similar to that in ring-banded poly(ethylene adipate) (PEA) spherulites crystallized at T_c = 28 °C, as earlier reported in the literature [1], and these periodically-grating PEA ring bands can display the nature of common bio-photonic crystals [40].

Obviously, from the in-situ monitoring from nucleation to final impingement for Type-1 and Type-2 banded PNT spherulties, the growth processes are composed of two stages. At the early age, sheaf-like nuclei, accompanied with a slanted 45°-angle, initiate at nearly two hours after quenching from T_{max} to T_c; then, polymer branches start to grow asymetrically from the two ends of nuclei-sheaves. Growth from the nuclei takes place by lengthening radially and branches evolve into fan-like sprays, which first widen and extend in the radial direction (i.e., ridge region on the top surface), then the tail-ends of the branches suddenly taper to bend down and precipitate to form a valley region. Subsequently, a new cycle starts and repeats in a similar manner until there is complete drainage of all molten species. In each cycle, the valley crystals are followed by a second-cycle growth, which continues periodically to form repetitive ring-banded PNT spherulites, whose crystal-aggregated patterns tend to be guided by the initial nucleus geometries, which in turn are influenced by kinetics parameters such as T_c and T_{max}.

4. Conclusions

By combining analyses of in-situ POM, AFM, and SEM analyses, this work aimed to probe the mechanisms of PNT displaying multiple types of assembly periodicity from nucleation to final packing into aggregated spherulites. Growth rates and the initial nuclei morphology until the subsequent spherulitic morphology were captured during in-situ crystallization on PNT specimens at various T_c after quenching from T_{max}. Initial morphologies of nuclei were analyzed with respect to final diversified periodic assemblies. Kinetic analyses alone cannot fully explain why PNT could form dual types of ring-banded morphology under a same thermal condition. By in-situ monitoring the entire crystallization process from initial nucleation until growth termination, we were able to clearly clarify the responsible causes. AFM and SEM results were used to expound the top-surface and interior lamellar arrangement of fully grown Type-1 and Type-2 spherulites. Furthermore, the nucleus region of fully grown Type-1 banded spherulites was exposed to show highly asymmetric sheaf-like textures, indicating that the nuclei for Type-1 ring bands do differ from those for Type-2.

Co-existence of dual types of banded PNT spherulites is present in PNT film specimens when crystallized at a series of T_c ranging from 60 to 85 °C. Growth processes from initial nucleation until fully-grown crystal entities of these two types of banded spherulites were monitored and analyzed using in-situ POM-CCD. Upon heating to various T_{max} (110–140 °C) and holding for 2 min at molten states prior to quenching to isothermal T_c = 75, 80 or 85 °C, relative fractions of Type-1 vs. Type-2 bands could vary significantly. The percentage (by volume or number) of Type-1 increases with higher T_{max}, suggesting that higher T_{max} is favorable for Type-1 but unfavorable for formation of Type-2 bands; for the Type-2 banded PNT spherulites, the changing tendency is just opposite to that of Type-1. For the Type-1 banded PNT spherulites, the initial nuclei are stick-like and have a highly asymmetrical sheaf-like shape. In fully grown Type-1 PNT banded spherulites, the sheaf-like nuclei are also clearly revealed inside the interior center of the spherulite; in addition, the interior lamellae grow asymmetrically in two directions along the nuclei with alternatively perpendicular orientation leading to a shell structure in the final Type-1 bands. In contrast, Type-2 PNT spherulites, which initially assumed a round nuclei shape, after the growing process still retain symmetrically rounded characteristics. The relative percentage of Type-1 bands always out-numbers that of Type-2. This work has shed light that different nucleation geometry and crystallization parameters collectively lead to development and evolution of multiple types of banded PNT spherulites with different relative fractions.

Author Contributions: Formal analysis, C.-H.T.; investigation, C.-H.T.; data curation, G.L. and S.N.; writing—original draft preparation, E.M.W.; writing—review and editing, E.M.W.; project administration, E.M.W.; funding acquisition, E.M.W. All authors have read and agreed to the published version of the manuscript.

Funding: This work was financially supported by a basic research grant (MOST-110-2811-E-006-509-MY2) for two consecutive years from Taiwan Ministry of Science and Technology (MOST), to which the authors express their gratitude.

Institutional Review Board Statement: Not applicable.

Informed Consent Statement: Not applicable.

Data Availability Statement: Not applicable.

Acknowledgments: SN is thankful to Taiwan's Ministry of Science and Technology for Postdoctoral Fellowship.

Conflicts of Interest: The authors declare no conflict of interest.

References

1. Woo, E.M.; Wang, L.-Y.; Nurkhamidah, S. Crystal lamellae of mutually perpendicular orientations by dissecting onto interiors of poly(ethylene adipate) spherulites crystallized in bulk form. *Macromolecules* **2012**, *45*, 1375–1383. [CrossRef]
2. Lugito, G.; Woo, E.M. Interior lamellar assembly in correlation to top-surface banding in crystallized poly(ethylene adipate). *Cryst. Growth Des.* **2014**, *14*, 4929–4936. [CrossRef]
3. Wang, L.Y.; Lugito, G.; Woo, E.M.; Wang, Y.H. Phase behavior, polymorphism and spherulite morphology in Poly(1,4-butylene adipate) interacting with two structurally similar acrylic polymers. *Polymer* **2012**, *53*, 3815–3826. [CrossRef]
4. Keith, H.D.; Padden, F.J. Banding in polyethylene and other spherulites. *Macromolecules* **1996**, *29*, 7776–7786. [CrossRef]
5. Sasaki, S.; Sakaki, Y.; Takahara, A.; Kajiyama, T. Microscopic lamellar organization in high-density polyethylene banded spherulites studied by scanning probe microscopy. *Polymer* **2002**, *43*, 3441–3446. [CrossRef]
6. Ho, R.M.; Ke, K.Z.; Chen, M. Crystal structure and banded spherulite of poly(trimethylene terephthalate). *Macromolecules* **2000**, *33*, 7529–7537. [CrossRef]
7. Xue, M.L.; Sheng, J.; Yu, Y.L.; Chuah, H.H. Nonisothermal crystallization kinetics and spherulite morphology of poly(trimethylene terephthalate). *Eur. Polym. J.* **2004**, *40*, 811–818. [CrossRef]
8. Wu, P.L.; Woo, E.M. Correlation between melting behavior and ringed spherulites in poly(trimethylene terephthalate). *J. Polym. Sci. Part B Polym. Phys.* **2002**, *41*, 80–93. [CrossRef]
9. Lugito, G.; Woo, E.M. Three types of banded structures in highly birefringent poly(trimethylene terephthalate) spherulites. *J. Polym. Sci. Part B Polym. Phys.* **2016**, *54*, 1207–1216. [CrossRef]
10. Lugito, G.; Woo, E.M. Novel approaches to study the crystal assembly in banded spherulites of poly(trimethylene terephthalate). *CrystEngComm* **2016**, *18*, 6158–6165. [CrossRef]
11. Lugito, G.; Woo, E.M.; Chuang, W.-T. Interior Lamellar Assembly and Optical Birefringence in Poly(trimethylene terephthalate) Spherulites: Mechanisms from Past to Present. *Crystals* **2017**, *7*, 56. [CrossRef]
12. Yen, K.C.; Woo, E.M.; Tashiro, K. Microscopic fourier transform infrared characterization on two types of spherulite with polymorphic crystals in poly(heptamethylene terephthalate). *Macromol. Rapid Commun.* **2010**, *31*, 1343–1347. [CrossRef] [PubMed]
13. Chen, Y.F.; Woo, E.M.; Li, S.H. Dual types of spherulites in poly (octamethylene terephthalate) confined in thin-film growth. *Langmuir* **2008**, *24*, 11880–11888. [CrossRef] [PubMed]
14. Woo, E.M.; Chen, Y.F. Single- and double-ring spherulites in poly(nonamethylene terephthalate). *Polymer* **2009**, *50*, 4706–4717. [CrossRef]
15. Chen, Y.F.; Woo, E.M. Annular multi-shelled spherulites in interiors of bulk-form Poly(nonamethylene terephthalate). *Macromol. Rapid Commun.* **2009**, *30*, 1911–1916. [CrossRef]
16. Woo, E.M.; Nurkhamidah, S.; Chen, Y.F. Surface and interior views on origins of two types of banded spherulites in poly(nonamethylene terephthalate). *Phys. Chem. Chem. Phys.* **2011**, *13*, 17841–17851. [CrossRef]
17. Woo, E.M.; Nurkhamidah, S. Surface Nanopatterns of Two Types of Banded Spherulites in Poly(nonamethylene terephthalate) Thin Films. *J. Phys. Chem. B* **2012**, *116*, 5071–5079. [CrossRef] [PubMed]
18. Lugito, G.; Woo, E.M.; Chang, S.-M. Periodic extinction bands composed of all flat-on lamellae in poly(dodecamethylene terephthalate) thin films crystallized at high temperatures. *J. Polym. Sci. Part B Polym. Phys.* **2017**, *55*, 601–611. [CrossRef]
19. Nagarajan, S.; Woo, E.M. Unique Optical Periodicity Assembly of Discrete Dendritic Lamellae and Pyramidal Single Crystals in Poly(ε-caprolactone). *ACS Appl. Mater. Interfaces* **2021**, *13*, 41200–41208. [CrossRef]
20. Nagarajan, S.; Woo, E.M. Three-dimensional periodic architecture in Poly(ε-caprolactone) crystallized in bulk aggregates. *Polymer* **2020**, *210*, 123059. [CrossRef]
21. Nagarajan, S. Lamellar Assembly Mechanism on Dendritic Ring-Banded Spherulites of Poly(ε-caprolactone). *Macromol. Rapid Commun.* **2021**, *42*, 2100359. [CrossRef] [PubMed]
22. Kossack, W.; Kremer, F. Banded spherulites and twisting lamellae in poly–ε–caprolactone. *Colloid Polym. Sci.* **2019**, *297*, 771–779. [CrossRef]
23. Mamun, A.; Bazuin, C.G.; Prud'Homme, R.E. Morphologies of various polycaprolactone/polymer blends in ultrathin films. *Macromolecules* **2015**, *48*, 1412–1417. [CrossRef]
24. Toda, A.; Taguchi, K.; Kajioka, H. Growth of banded spherulites of poly(ε-caprolactone) from the blends: An examination of the modeling of spherulitic growth. *Polymer* **2012**, *53*, 1765–1771. [CrossRef]
25. Li, Y.; Huang, H.; Wang, Z.; He, T. Tuning radial lamellar packing and orientation into diverse ring-banded spherulites: Effects of structural feature and crystallization condition. *Macromolecules* **2014**, *47*, 1783–1792. [CrossRef]
26. Li, Y.; Huang, H.; He, T.; Wang, Z. Band-to-nonband transition into unique poly(ε-caprolactone) crystals by modulating the interplay of diffusion and growth. *ACS Macro Lett.* **2012**, *1*, 718–722. [CrossRef]
27. Yam, W.Y.; Ismail, J.; Kammer, H.W.; Schmidt, H.; Kummerlöwe, C. Polymer blends of poly(ε-caprolactone) and poly(vinyl methyl ether)—Thermal properties and morphology. *Polymer* **1999**, *40*, 5545–5552. [CrossRef]
28. Keith, H.D.; Padden, F.J. The optical behavior of spherulites in crystalline polymers. Part I. Calculation of theoretical extinction patterns in spherulites with twisting crystalline orientation. *J. Polym. Sci.* **1959**, *39*, 101–122. [CrossRef]
29. Keith, H.D.; Padden, F.J. The optical behavior of spherulites in crystalline polymers. Part II. The growth and structure of the spherulites. *J. Polym. Sci.* **1959**, *39*, 123–138. [CrossRef]
30. Keller, A. Investigations on banded spherulites. *J. Polym. Sci.* **1959**, *39*, 151–173. [CrossRef]

31. Lustiger, A.; Lotz, B.; Duff, T.S. The morphology of the spherulitic surface in polyethylene. *J. Polym. Sci. Part B Polym. Phys.* **1989**, *27*, 561–579. [CrossRef]
32. Lotz, B.; Cheng, S.Z.D. A critical assessment of unbalanced surface stresses as the mechanical origin of twisting and scrolling of polymer crystals. *Polymer* **2005**, *46*, 577–610. [CrossRef]
33. Tu, C.H.; Woo, E.M.; Lugito, G. Structured growth from sheaf-like nuclei to highly asymmetric morphology in poly(nonamethylene terephthalate). *RSC Adv.* **2017**, *7*, 47614–47618. [CrossRef]
34. Weber, J.; Petrović, D.; Strodel, B.; Smits, S.H.J.; Kolkenbrock, S.; Leggewie, C.; Jaeger, K.-E. Interaction of carbohydrate-binding modules with poly(ethylene terephthalate). *Appl. Microbiol. Biotechnol.* **2019**, *103*, 4801–4812. [CrossRef]
35. Tu, C.-H.; Woo, E.M.; Nagarajan, S.; Lugito, G. Sophisticated dual-discontinuity periodic bands of poly(nonamethylene terephthalate). *CrystEngComm* **2021**, *23*, 892–903. [CrossRef]
36. Nagarajan, S.; Woo, E.M. Periodic Assembly of Polyethylene Spherulites Re-Investigated by Breakthrough Interior Dissection. *Macromol. Rapid Commun.* **2021**, *42*, 2000708. [CrossRef]
37. Woo, E.M.; Lugito, G.; Chang, S.-M. Three-dimensional interior analyses on periodically banded spherulites of poly(dodecamethylene terephthalate). *CrystEngComm* **2018**, *20*, 1935–1944. [CrossRef]
38. Woo, E.M.; Lee, M.-S. Crystallization in arylate polyesters to periodically ringed assembly. *Polym. Cryst.* **2018**, *1*, e10018. [CrossRef]
39. Yeh, Y.T.; Woo, E.M. Anatomy into interior lamellar assembly in nuclei-dependent diversified morphologies of poly(L-lactic acid). *Macromolecules* **2018**, *51*, 7722–7733. [CrossRef]
40. Woo, E.M.; Yen, K.C.; Yeh, Y.T.; Wang, L.Y. Biomimetically structured lamellae assembly in periodic banding of poly(ethylene adipate) crystals. *Macromolecules* **2018**, *51*, 3845–3854. [CrossRef]